Table 1. GRNs built in this study.

network type	study	note	N
tissue	Stelpflug et al. 2016	B73	93
	Walley et al. 2016	B73	23
	Zhou et al. 2018	B73	23
		Mo17	23
		BxM	23
	Yi et al. 2019	seed dev	31
	Tissue Atlas	combined	247
genotype	Eichten et al. 2013	seedling_leaf3	62
	Fu et al. 2013	kernel	368
	Hirsch et al. 2014	seedling	503
	Leiboff et al. 2015	SAM	383
	Lin et al. 2017	ear	26
		root	27
		shoot	27
		tassel	26
		SAM	27
	Kremling et al. 2018	GRoot	201
		GShoot	271
		Kern	226
		L3Base	254
		L3Tip	257
		LMAD	199
		LMAN	249
	Shaefer et al. 2018	root_GCN	48
	Huang et al. 2018	leaf	394
		root	176
		SAM	406
		seed	159
	Mazaheri et al. 2019	seedling	453
	Li et al. 2019	endosperm	121
		internode	77
		leaf	84
		root	84
		shoot	85
		seedling	169
tissue*genotype	Lin et al. 2017	5*27	133
	Kremling et al. 2018	7*237	1657
	Huang et al. 2018	4*300	1136
	Zhou et al. 2018	23*3	73
	Li et al. 2019	6*103	620
ril	Li et al. 2013	B73 x Mo17	107
	Baute et al. 2016	MAGIC	102
	Baute et al. 2015	B73 x H99	106
	Wang et al. 2018	W22 x Teosinte	617

Table S1. TF knockout mutant RNA-Seq datasets used in this study.

TF alias	TF name	TF ID	Study	Accession	Tissue	N
kn1	knotted1	Zm00001d033859	bolduc2012	PRJNA168086	meristem	10
cle7	clavata3/esr-related7	GRMZM2G372364		PRJNA494874	ear tip	4
rbm48	RNA binding motif protein 48	Zm00001d054077		PRJNA485828	endosperm	16
dek42	RNA binding motif protein 48	Zm00001d054077		PRJNA485820	kernel	6
mads47	MADS-transcription factor 47	Zm00001d046053		PRJNA289143	kernel	2
ufo1	unstable factor for orange1	Zm00001d000009	wittmeyer2018	PRJNA483200	pericarp	27
rel2	ramosa1 enhancer locus2	Zm00001d024523	liu2018	PRJNA475209	tassel	6
o2	opaque2	Zm00001d018971	zhan2018	PRJNA471036	endosperm	6
o2_b	opaque2	Zm00001d018971	li2015	PRJNA262503	endosperm	2
bzip22	bZIP-transcription factor 22	Zm00001d021191	li2018	PRJNA449867	kernel	6
fl3	floury3	Zm00001d009292	li2017	PRJNA375801	endosperm	6
fea4	fasciated ear4	Zm00001d037317	pautler2015	PRJNA262781	ear primordia	6
liguleless	liguleless1	Zm00001d002005	johnston2014	PRJNA260793	leaf primordia	24
nkd	naked endosperm1	Zm00001d002654	gontarek2016	PRJNA260183	aleurone, endosperm	2
sk1	silkless ears1	Zm00001d002970		PRJNA483310	young V9 tassel	6
dek15	defective kernel15	Zm00001d052197		PRJNA494076	kernel	6
ra1	RAMOSA1	Zm00001d020430	Eveland2014	PRJNA219746	ear	10
ra2	RAMOSA2	Zm00001d039694	Eveland2014	PRJNA219746	ear	10
ra3	RAMOSA3	Zm00001d022193	Eveland2014	PRJNA219746	ear	10
P1	Pericarp Color1	Zm00001d028842	Morohashi2012	PRJNA167802	pericarp	6
hda101	RPD3 histone deacetylase homolog	Zm00001d053595	Yang2016	PRJNA305809	seed	6

Table S2. Natural variation datasets used for validation in this study.

author	study	condition	contrast	non-DE	DE1-2	DE2-4	DE4+	SPE
umn2014	stress	seedling cold	B73 vs B37	14,991	5,508	2,524	2,191	765
		seedling cold	B73 vs Oh43	13,985	6,013	2,955	2,226	800
		seedling control	B73 vs B37	11,868	7,131	3,468	2,551	961
		seedling control	B73 vs Oh43	12,804	6,395	3,213	2,545	1,022
		seedling heat	B73 vs B37	14,488	5,491	2,937	2,276	787
		seedling heat	B73 vs Oh43	13,304	5,931	3,249	2,568	927
weihmann2016	Colletotrichum infection	leaf	B73 vs GJ	6,263	7,349	3,982	2,814	1,339
waters2017	stress cis-trans	leaf3 cold	B73 vs Mo17	17,235	2,783	2,136	1,550	796
		leaf3 cold	B73 vs PH207	17,202	3,023	2,075	1,439	761
		leaf3 control	B73 vs Mo17	18,843	2,012	1,610	1,226	809
		leaf3 control	B73 vs PH207	19,148	1,868	1,447	1,239	798
		leaf3 heat	B73 vs Mo17	18,453	2,433	1,641	1,152	821
		leaf3 heat	B73 vs PH207	16,533	3,404	2,312	1,459	792
marcon2017	drought stress	root control	B73 vs Mo17	13,185	6,718	2,513	1,940	651
		root drought	B73 vs Mo17	13,828	6,370	2,347	1,864	598
baldauf2018	SPE	root1	B73 vs A554	14,789	5,809	2,346	1,978	845
		root1	B73 vs H84	14,118	6,607	2,417	1,793	832
		root1	B73 vs H99	13,739	6,725	2,521	1,886	896
		root1	B73 vs Mo17	13,533	6,851	2,497	1,975	911
		root1	B73 vs Oh43	13,572	6,839	2,484	1,945	927
		root1	B73 vs W64A	13,587	6,881	2,411	1,996	892
		root2	B73 vs A554	12,127	7,813	2,783	2,077	967
		root2	B73 vs H84	15,728	5,568	2,086	1,573	812
		root2	B73 vs H99	10,259	9,102	3,284	2,157	965
		root2	B73 vs Mo17	14,185	6,490	2,291	1,880	921
		root2	B73 vs Oh43	8,927	9,398	3,930	2,577	935
		root2	B73 vs W64A	11,262	8,504	3,024	2,058	919
		root3	B73 vs A554	12,628	7,527	2,649	2,003	960
		root3	B73 vs H84	13,350	7,061	2,636	1,891	829
		root3	B73 vs H99	11,305	8,578	2,865	2,136	883
		root3	B73 vs Mo17	12,659	7,721	2,574	1,894	919
		root3	B73 vs Oh43	13,539	6,965	2,408	1,977	878
		root3	B73 vs W64A	11,131	8,612	3,063	2,033	928
sun2018	mo17 genome	bract	B73 vs Mo17	19,008	832	980	1,192	702
		endosperm	B73 vs Mo17	18,841	1,021	1,240	1,016	596
		root	B73 vs Mo17	18,760	820	1,114	1,371	649
		seedling	B73 vs Mo17	19,416	661	850	980	807
		stem	B73 vs Mo17	18,669	887	1,130	1,164	864
zhou2018	B73 Mo17 atlas	auricle	B73 vs Mo17	14,944	3,885	2,596	2,091	860
		blade leaf	B73 vs Mo17	16,331	3,174	2,170	1,775	926
		coleoptile	B73 vs Mo17	18,653	2,392	1,389	1,367	575
		ear	B73 vs Mo17	18,838	2,425	1,213	1,095	805
		embryo	B73 vs Mo17	16,351	3,577	2,227	1,407	814
		endosperm14D	B73 vs Mo17	17,848	2,570	1,748	1,468	742
		endosperm27D	B73 vs Mo17	16,695	3,105	2,254	1,458	864
		flag leaf	B73 vs Mo17	16,090	3,146	2,329	1,898	913
		floret	B73 vs Mo17	17,037	3,259	1,977	1,342	761
		husk	B73 vs Mo17	16,723	3,362	1,809	1,605	877
		internode	B73 vs Mo17	13,644	4,273	2,844	2,653	962
		kernel	B73 vs Mo17	17,590	2,946	1,734	1,362	744
		radicle root	B73 vs Mo17	18,120	2,346	1,764	1,501	645
		root	B73 vs Mo17	17,334	2,883	1,844	1,499	816
		seed imbibed	B73 vs Mo17	12,068	5,342	3,606	2,626	734
		seedling leaf	B73 vs Mo17	16,245	2,938	2,286	2,079	828
		seedling meristem	B73 vs Mo17	19,207	1,923	1,249	1,235	762
		seedling root	B73 vs Mo17	18,842	2,009	1,631	1,180	714
		sheath	B73 vs Mo17	15,209	3,885	2,633	1,810	839
		silk	B73 vs Mo17	15,378	3,577	2,303	2,152	966
		spikelet	B73 vs Mo17	17,984	2,736	1,589	1,209	858
		tassel	B73 vs Mo17	15,594	3,856	2,435	1,677	814
		tassel stem	B73 vs Mo17	12,564	4,625	3,512	2,652	1,023

Table S3. GRN-predicted TFs supported by trans-eQTL hotspots.

ID	Support eQTL study	Support GRN	TF Annotation	Target enrichment
Zm00001d002075	li2013	li2013, baute2015	Floral homeotic protein APETALA 2	
Zm00001d003162	li2013	tissue atlas, huang2018, li2013	Zinc finger protein CONSTANS-LIKE 5	(28) rRNA processing; (16) photosystem II assembly; (16) photosynthesis light reactions; (6) phenylpropanoid biosynthesis; (5) chloroplast organization
Zm00001d004497	wang2018	baute2015, wang2018	C2H2-like zinc finger protein	
Zm00001d005016	liu2017,wang2018	baute2016, baute2015, baute2016, baute2015	WRI1 transcription factor1	
Zm00001d006578	li2013	li2013, baute2015	Transcription factor bHLH130	(24) L-alanine degradation II (to D-lactate)
Zm00001d006677	li2013	huang2018, li2013	Protein BRASSINAZOLE-RESISTANT 1	
Zm00001d006701	li2013	li2013, baute2015	GRAS transcription factor	
Zm00001d010060	liu2017	baute2015, wang2018	BEL1-like homeodomain protein 9	
Zm00001d010785	liu2017	li2013, baute2015	Putative GATA transcription factor family protein	
Zm00001d012605	wang2018	li2013, baute2015	MRP interacting1	
Zm00001d015412	wang2018	li2013, baute2015	sequence-specific DNA binding transcription factors	(18) suberin monomers biosynthesis; (13) L-glutamate degradation IV
Zm00001d015743	wang2018	tissue atlas, zhou2018	Transcription factor HY5	(73) thylakoid membrane organization; (10) transmembrane transport; (9) positive regulation of transcription, DNA-templated; (8) chloroplast organization
Zm00001d017788	wang2018	li2013, baute2015	Dof zinc finger protein DOF2.1	
Zm00001d018465	wang2018	li2013, baute2015		
Zm00001d019230	wang2018	baute2016, baute2015	sister of indeterminate spikelet1	
Zm00001d020019	liu2017,wang2018	li2013, baute2016, baute2015, li2013, baute2015	Protein PHR1-LIKE 3	
Zm00001d020043	liu2017	li2013, baute2015	Ethylene-responsive transcription factor ERF117	
Zm00001d020408	wang2018	li2013, baute2015	Typical P-type R2R3 Myb protein	
Zm00001d021403	wang2018	li2013, baute2015	indeterminate1 domain7	(9) sporopollenin precursors biosynthesis; (8) sucrose degradation II (sucrose synthase)
Zm00001d024041	liu2017,wang2018	li2013, baute2016, baute2015, li2013, baute2015	bZIP transcription factor 16	
Zm00001d024230	liu2017,wang2018	li2013, baute2015, li2013, baute2015	Nuclear transcription factor Y subunit C-2	
Zm00001d024268	li2013,liu2017	li2013, baute2015, li2013, baute2015	NAC domain-containing protein 21/22	
Zm00001d026147	wang2018	li2013, baute2015	plant color component at R1	(57) anthocyanin biosynthesis; (19) flavonoid biosynthesis (in equisetum)

Zm00001d029963	wang2018	baute2015, wang2018	myb-like transcription factor family protein	
Zm00001d030028	wang2018	li2013, baute2016	myc transcription factor7	(28) regulation of transcription, DNA-templated; (20) cutin biosynthesis; (14) regulation of transcription, DNA-templated; (13) response to wounding; (9) jasmonic acid biosynthesis; (8) response to wounding; (7) phospholipases
Zm00001d030727	wang2018	li2013, baute2015	Dof zinc finger protein DOF2.2	(11) microtubule cytoskeleton organization
Zm00001d030907	wang2018	li2013, baute2015	B3 domain-containing protein	(7) xylose degradation I
Zm00001d031561	wang2018	baute2015, wang2018	Transcription factor bHLH62	(31) response to wounding; (12) pyrimidine ribonucleosides salvage II; (8) protein targeting to membrane
Zm00001d031665	wang2018	baute2016, baute2015	Transcription factor bHLH137	(20) triacylglycerol degradation
Zm00001d033898	wang2018	tissue atlas, baute2015	BEL1-like homeodomain protein 4	(34) Calvin-Benson-Bassham cycle; (24) rRNA processing; (7) photosynthesis light reactions; (6) photosystem II assembly
Zm00001d035084	li2013	baute2016, baute2015	Putative NAC domain transcription factor superfamily protein	(6) cellulose biosynthesis
Zm00001d035195	li2013	tissue atlas, huang2018	Protein LSD1	
Zm00001d036214	li2013	li2013, baute2016	B-box zinc finger protein 22	(19) glycolysis I (from glucose 6-phosphate)
Zm00001d041277	liu2017	li2013, baute2016	Putative axial regulator YABBY 2	
Zm00001d044168	li2013	li2013, baute2015	Heat stress transcription factor C-1	
Zm00001d044260	li2013	li2013, baute2015	C3H-type transcription factor	
Zm00001d044355	li2013,wang2018	huang2018, li2013, baute2015, wang2018, li2013, baute2015	B3 domain-containing protein	(5) triacylglycerol degradation
Zm00001d044538	li2013	zhou2018, huang2018		(18) triacylglycerol degradation; (8) regulation of transcription by RNA polymerase II
Zm00001d045581	liu2017	li2013, baute2016, baute2015	Putative MYB DNA-binding domain superfamily protein	
Zm00001d045661	liu2017	li2013, baute2015	Zinc finger protein CONSTANS-LIKE 16	(46) photosynthesis, light harvesting in photosystem I; (19) photosynthesis light reactions; (17) rRNA processing; (7) response to cold; (6) photosynthesis
Zm00001d046323	liu2017	li2013, baute2015		
Zm00001d046405	liu2017	baute2016, baute2015	Putative homeodomain-like transcription factor superfamily protein	(66) isopentenyl diphosphate biosynthetic process, methylerythritol 4-phosphate pathway; (59) thylakoid membrane organization; (21) positive regulation of transcription, DNA-templated; (14) tetrapyrrole biosynthesis I (from glutamate); (12) RNA modification; (12) 3,8-divinyl-chlorophyllide *a* biosynthesis I (aerobic, light-dependent); (8) photosynthesis light reactions

Zm00001d046441	liu2017	li2013, baute2016, baute2015	FAR1-domain family sequence	
Zm00001d047519	wang2018	li2013, baute2015	basic leucine-zipper 52	
Zm00001d047563	wang2018	li2013, baute2015	ethylene insensitive-like1	(6) translation
Zm00001d047968	wang2018	li2013, baute2015	Zinc finger protein 1	(20) gluconeogenesis I
Zm00001d050781	wang2018	li2013, baute2015	Auxin response factor 1	
Zm00001d052847	wang2018	li2013, baute2016	Putative WRKY DNA-binding domain superfamily protein	
Zm00001d053124	li2013	tissue atlas, zhou2018, li2019, huang2018	myb domain protein 60	(36) thylakoid membrane organization; (27) isopentenyl diphosphate biosynthetic process, methylerythritol 4-phosphate pathway; (15) chloroplast organization; (12) photosynthesis, light harvesting in photosystem I; (11) Calvin-Benson-Bassham cycle; (6) response to cytokinin
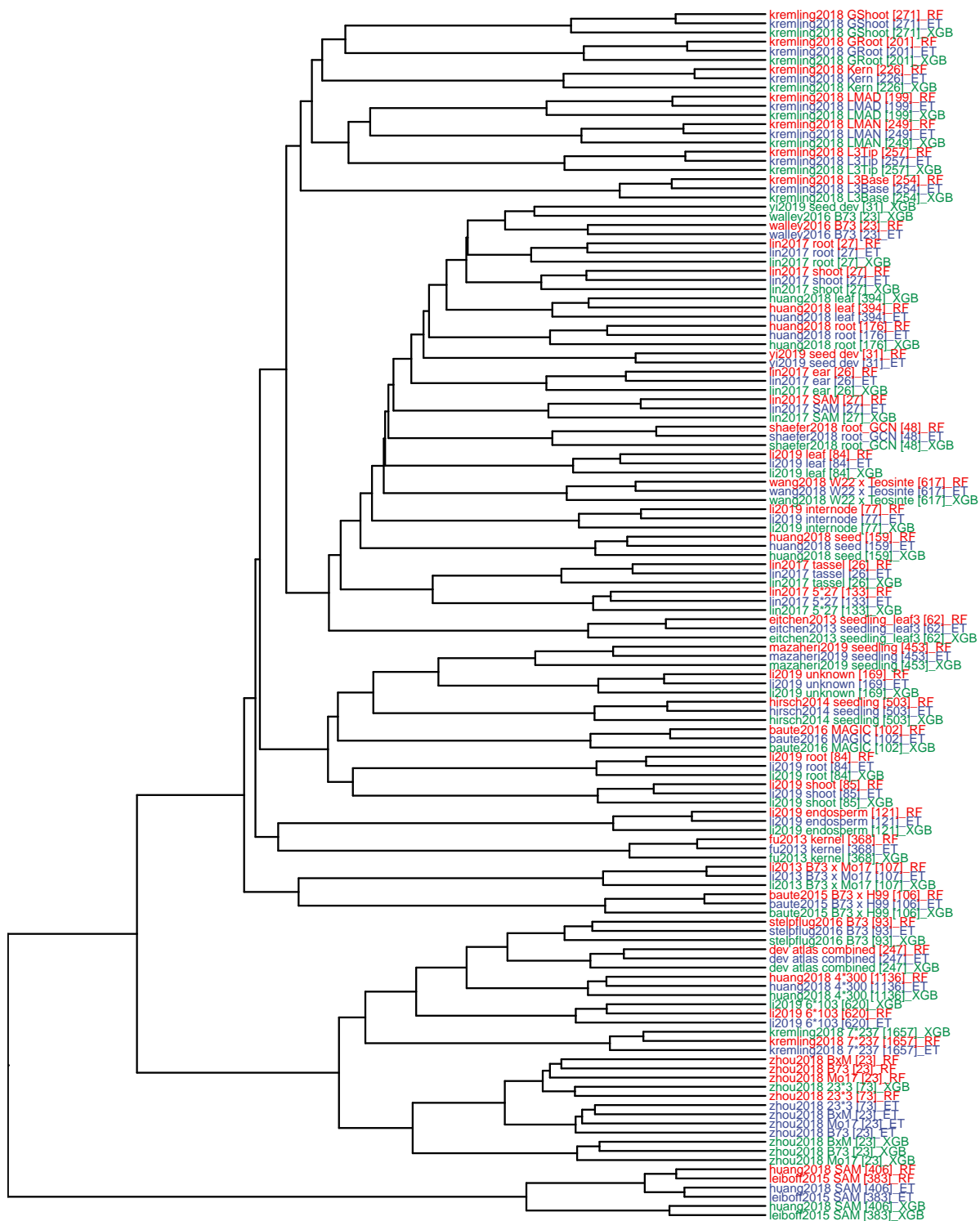
Figure S1. Hierarchical clustering of 132 GRNs (44 expression dataset * 3 methods). Each of the three regression-based method (random forest, extra trees, gradient boosted) was used to build a network for each RNA-Seq dataset. Pairwise distance between networks was determined by taking the top 100,000 TF-target predictions from each network and calculating the proportion of shared (common) predictions (using 'dist()'

function in R with additional argument 'method=binary'). Hierarchical clustering was then performed based on the cross-network pairwise distance matrix using "ward.D" option.
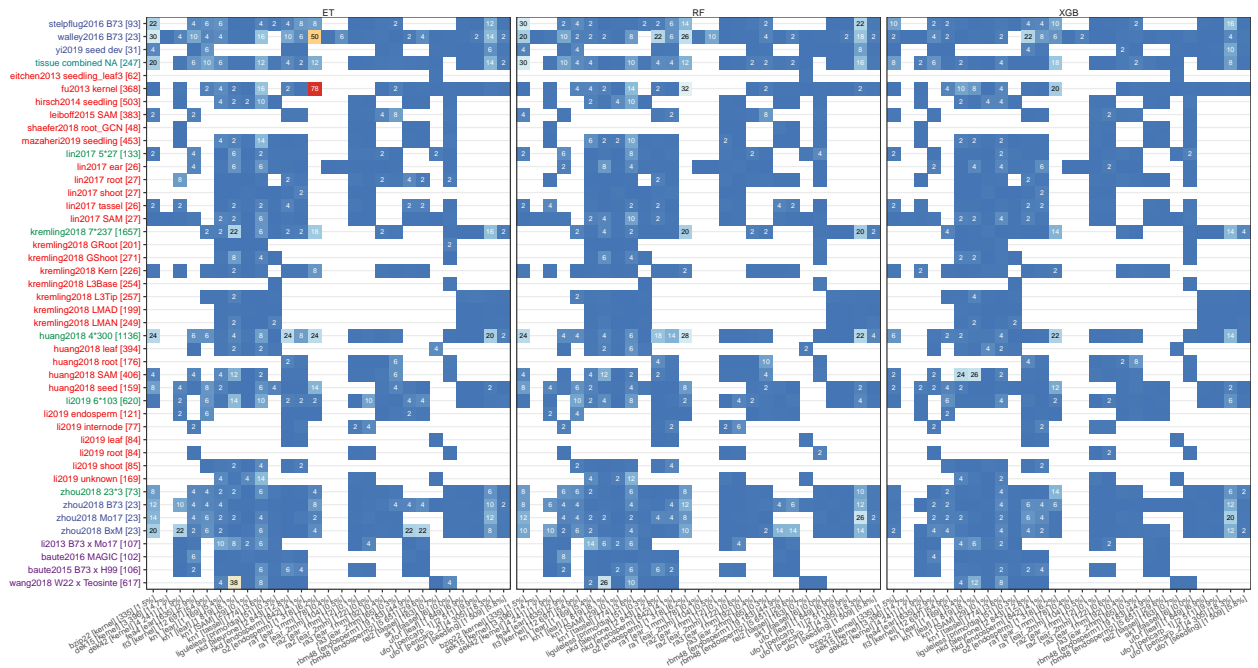
Figure S1b.

Figure S3. Comparison of GRNs built with different methods using supports from TF knockout mutant RNA-Seq data.
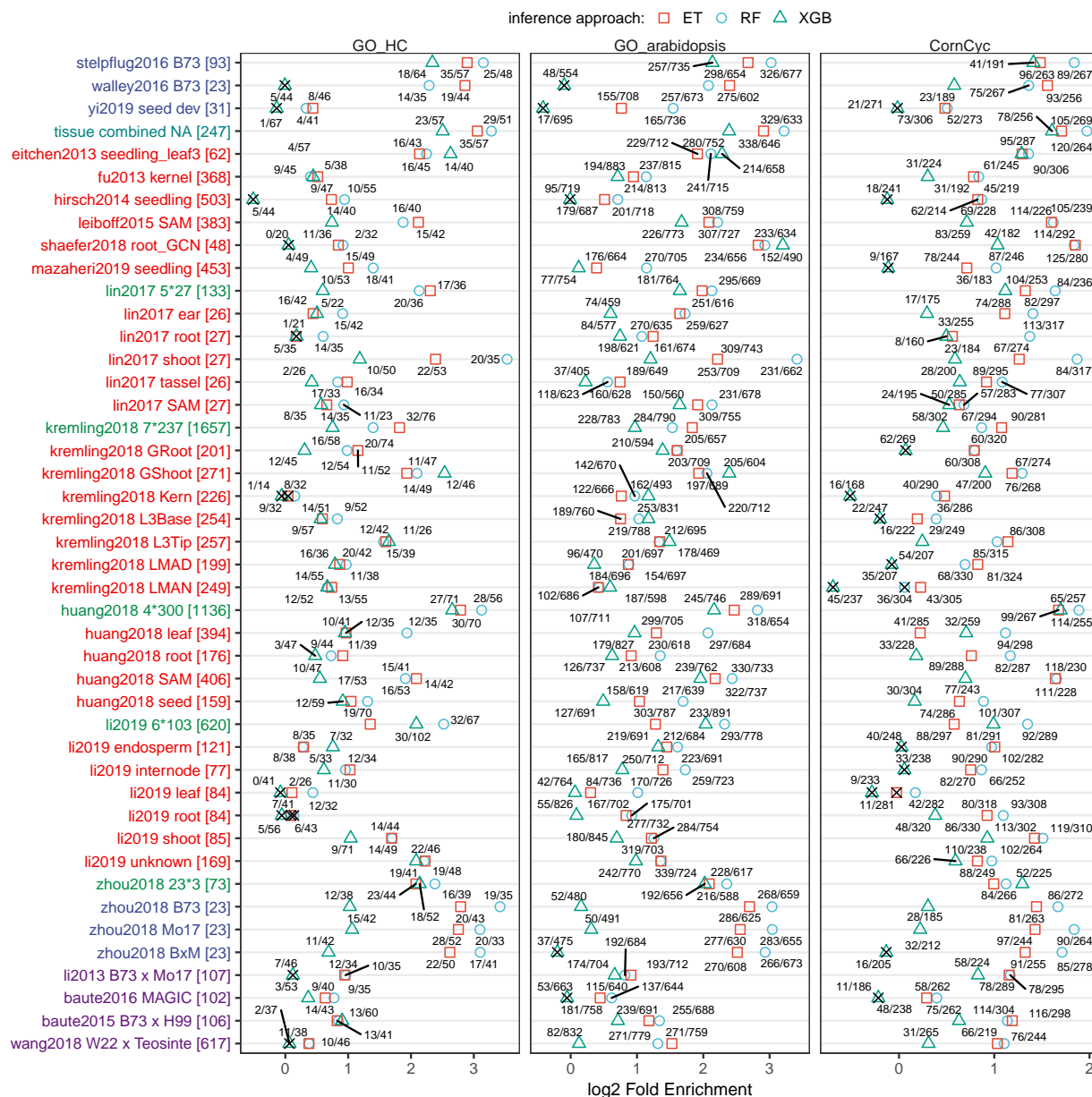
Figure S4. Comparison of GRNs built with different methods using supports from TF knockout mutant RNA-Seq data.
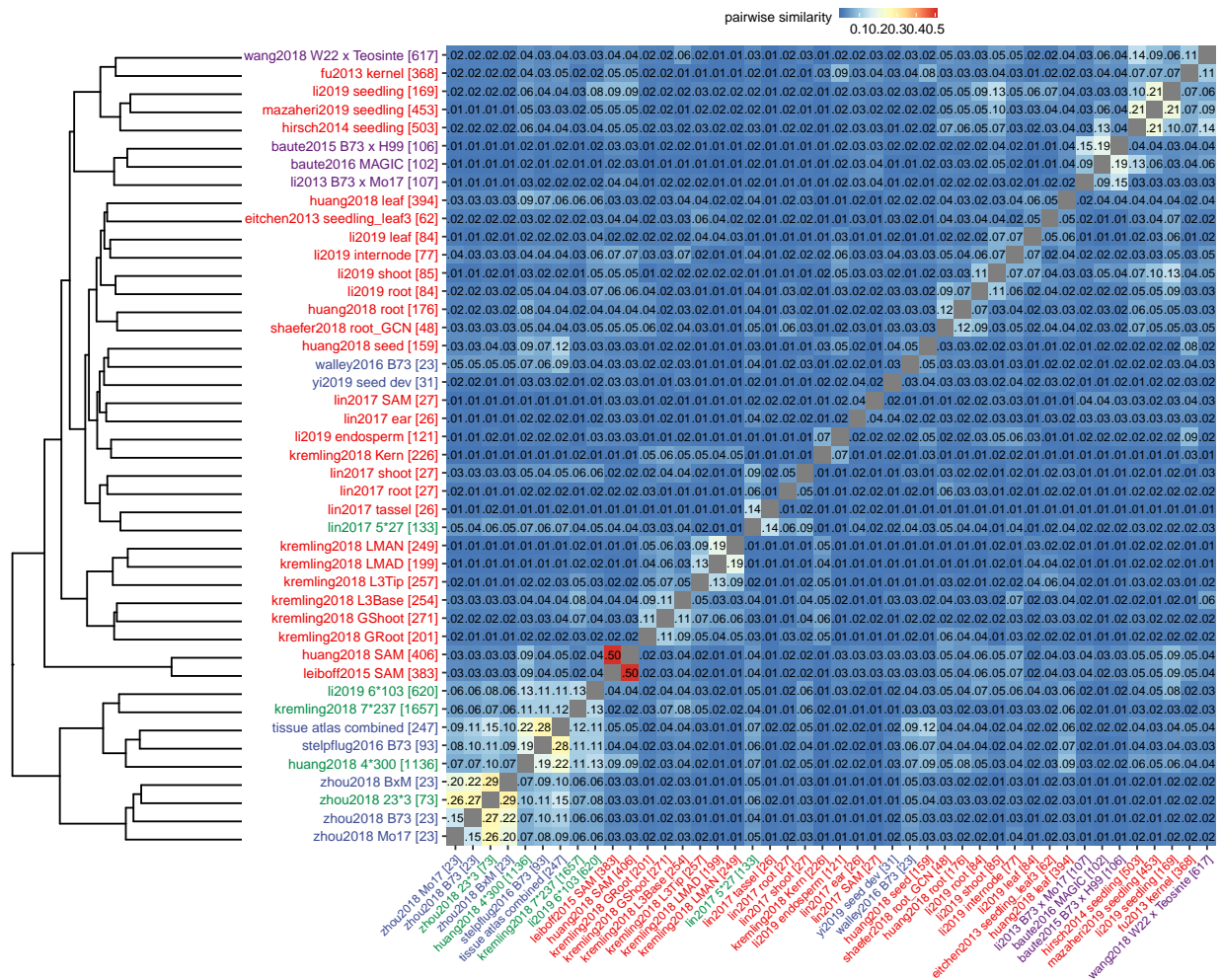
Figure 1. Hierarchical clustering of 44 GRNs. Pairwise distance between networks was determined by taking the top 100,000 TF-target predictions from each network and calculating the proportion of shared (common) predictions (using 'dist()' function in R with additional argument 'method=binary'). Hierarchical clustering was then performed based on the cross-network pairwise distance matrix using "ward.D" method.
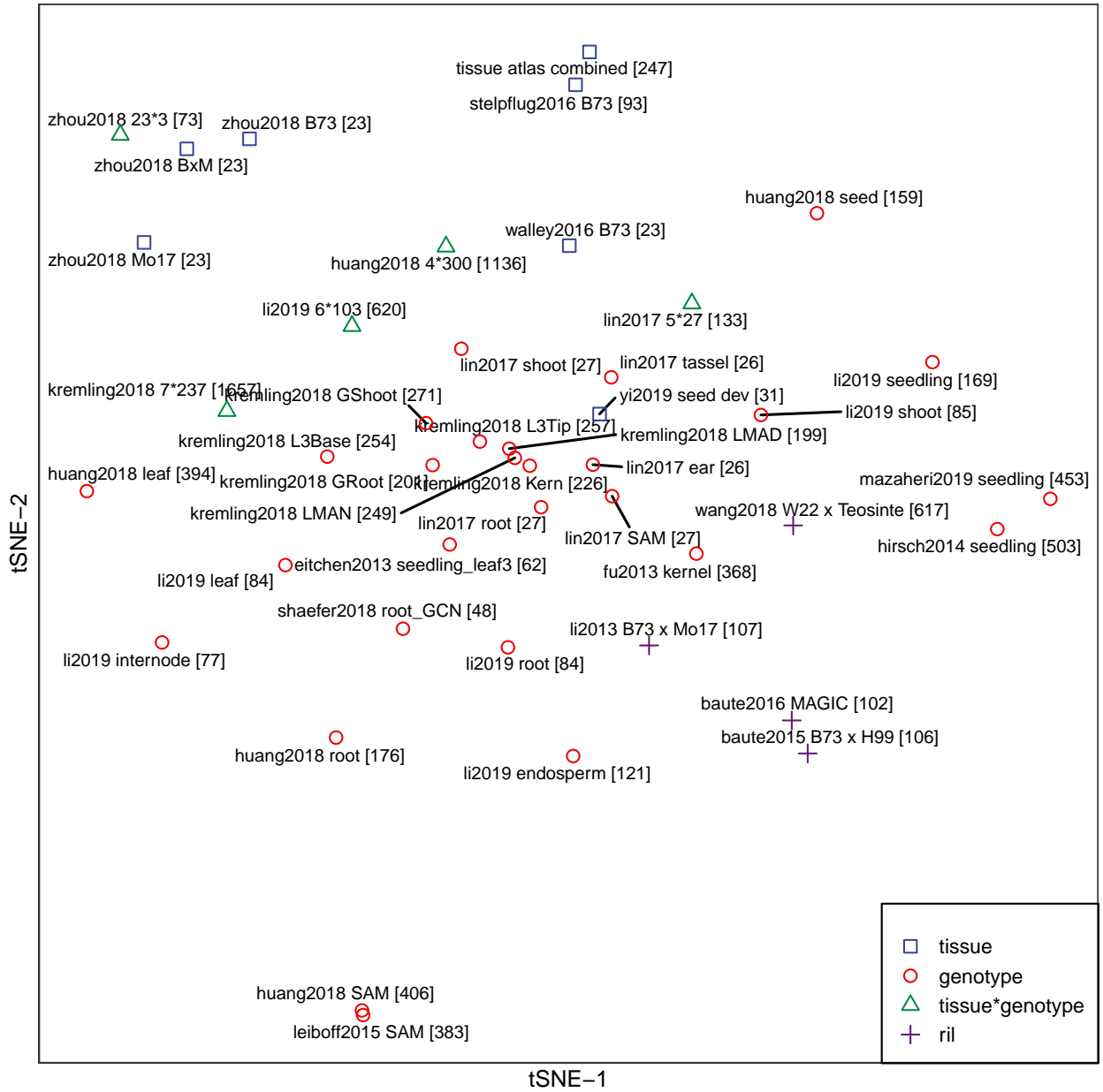
Figure S5. T-SNE clustering of 44 GRNs. Top 500,000 TF-target predictions were extracted from each network to perform t-SNE clustering using parameter "perplexing=9, permutation=2000".
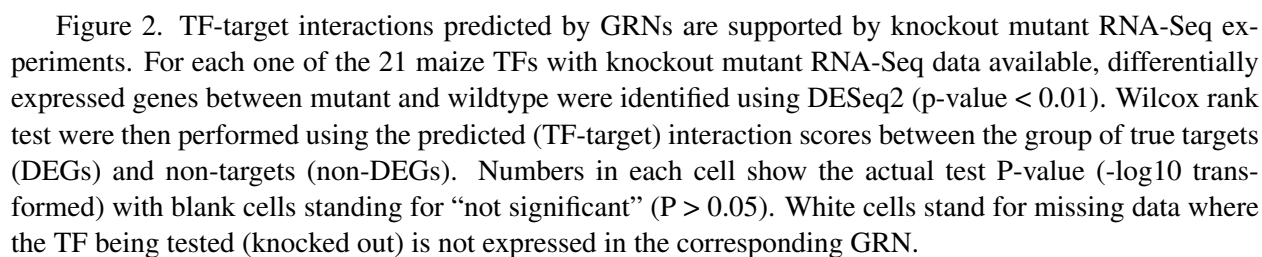
Figure 2. TF-target interactions predicted by GRNs are supported by knockout mutant RNA-Seq experiments. For each one of the 21 maize TFs with knockout mutant RNA-Seq data available, differentially expressed genes between mutant and wildtype were identified using DESeq2 (p-value < 0.01). Wilcox rank test were then performed using the predicted (TF-target) interaction scores between the group of true targets (DEGs) and non-targets (non-DEGs). Numbers in each cell show the actual test P-value (-log10 transformed) with blank cells standing for "not significant" (P > 0.05). White cells stand for missing data where the TF being tested (knocked out) is not expressed in the corresponding GRN.
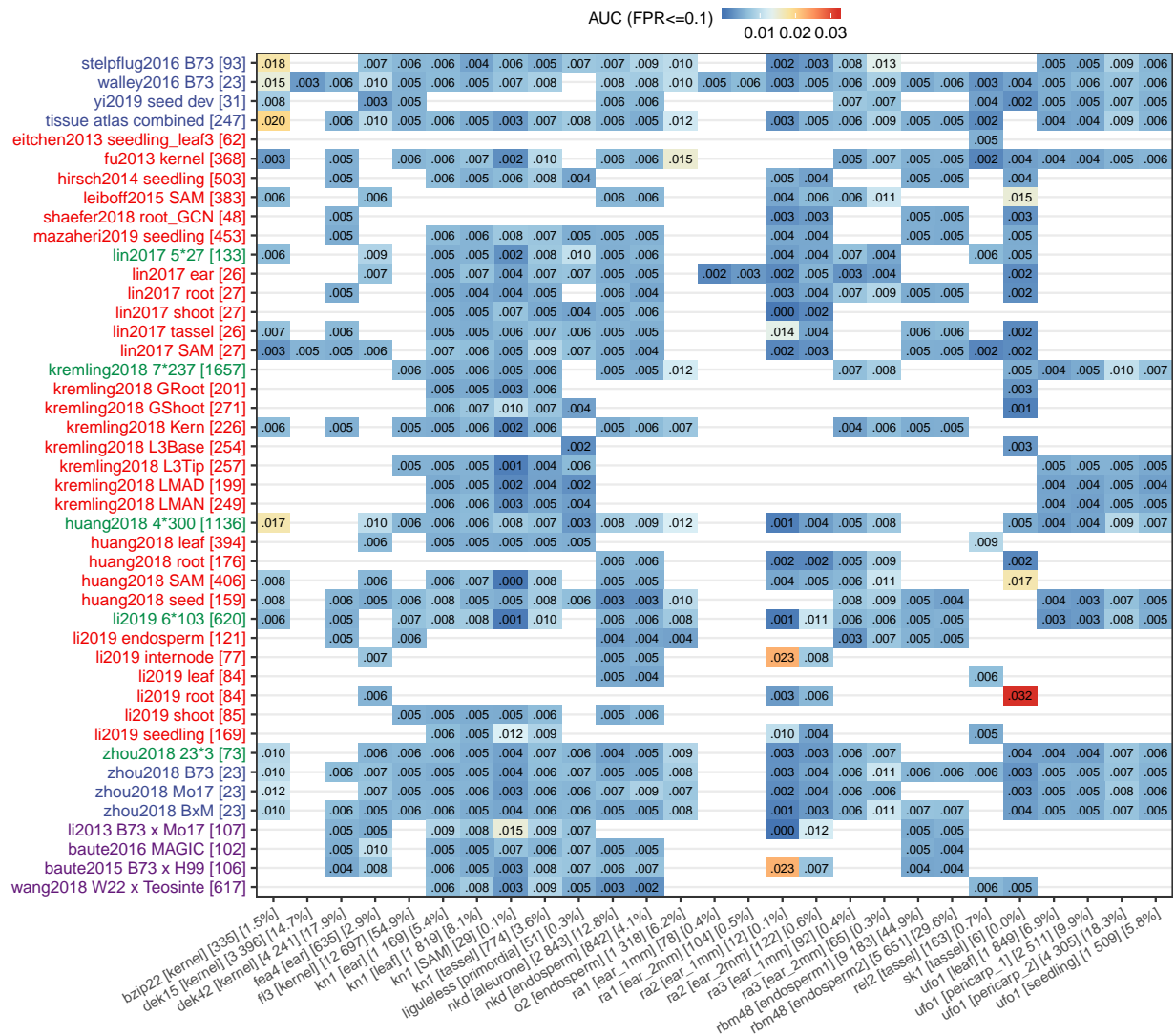
Figure S6. Area under receiver-operating characteristic curve (AUROC) evaluated for each GRN (until an False Positive Rate of 0.1 is reached) using support from 21 maize TF knockout mutants as ground truth. Differentially expressed genes between each TF knockout mutant and the wildtype were identified using DESeq2 (p-value < 0.01) and treated as ground truth to evaluate GRN performance. Numbers in each cell show the actual AUROC values with white cells indicating missing data (the TF being filtered from the expression matrix due to invariable expression).

The heatmap "AUC (FPR<=0.1)" with color scale 0.01 0.02 0.03. Columns: FunTFBS + motif + motif_CE [4 115], FunTFBS + motif [7 459], motif + motif_CE [37 699], motif [202 670].

Dataset	FunTFBS + motif + motif_CE [4 115]	FunTFBS + motif [7 459]	motif + motif_CE [37 699]	motif [202 670]
stelpflug2016 B73 [93]	.012	.002	.007	.005
walley2016 B73 [23]	.009	.007	.006	.006
yi2019 seed dev [31]	.016	.008	.009	.005
tissue atlas combined [247]	.018	.009	.011	.005
eitchen2013 seedling_leaf3 [62]	.012	.006	.006	.005
fu2013 kernel [368]	.009	.006	.008	.005
hirsch2014 seedling [503]	.015	.011	.011	.010
leiboff2015 SAM [383]	.012	.007	.008	.005
shaefer2018 root_GCN [48]	.007	.010	.007	.007
mazaheri2019 seedling [453]	.008	.006	.007	.005
lin2017 5*27 [133]	.006	.005	.005	.005
lin2017 ear [26]	.011	.006	.004	.006
lin2017 root [27]	.005	.005	.005	.005
lin2017 shoot [27]	.008	.008	.007	.006
lin2017 tassel [26]	.004	.006	.004	.006
lin2017 SAM [27]	.012	.007	.007	.006
kremling2018 7*237 [1657]	.008	.008	.007	.004
kremling2018 GRoot [201]	.012	.009	.005	.005
kremling2018 GShoot [271]	.020	.011	.008	.006
kremling2018 Kern [226]	.018	.008	.009	.005
kremling2018 L3Base [254]	.004	.009	.006	.006
kremling2018 L3Tip [257]	.008	.014	.010	.005
kremling2018 LMAD [199]	.017	.010	.007	.005
kremling2018 LMAN [249]	.006	.006	.005	.005
huang2018 4*300 [1136]	.011	.011	.009	.006
huang2018 leaf [394]	.008	.010	.006	.005
huang2018 root [176]	.010	.011	.007	.006
huang2018 SAM [406]	.013	.007	.009	.005
huang2018 seed [159]	.008	.005	.005	.006
li2019 6*103 [620]	.008	.005	.007	.007
li2019 endosperm [121]	.031	.017	.009	.005
li2019 internode [77]	.032	.013	.016	.007
li2019 leaf [84]	.011	.006	.005	.006
li2019 root [84]	.011	.010	.005	.005
li2019 shoot [85]	.017	.012	.010	.006
li2019 seedling [169]	.010	.003	.008	.005
zhou2018 23*3 [73]	.011	.005	.006	.005
zhou2018 B73 [23]	.010	.004	.006	.005
zhou2018 Mo17 [23]	.011	.005	.007	.005
zhou2018 BxM [23]	.010	.006	.007	.006
li2013 B73 x Mo17 [107]	.005	.007	.006	.005
baute2016 MAGIC [102]	.009	.008	.011	.007
baute2015 B73 x H99 [106]	.015	.004	.007	.005
wang2018 W22 x Teosinte [617]	.006	.006	.005	.007

Figure S7. Evaluation of constructed GRNs using four sets of predicted TF-target interactions based on TF-binding site motif, conserved element of TFBS motif or FunTFBS. There are 202,670 "motif"-based predictions, 37,699 predictions based on motif and cross-species conservation, 7,459 predictions based on motif and FunTFBS as well as 4,115 predictions based on all three evidences.
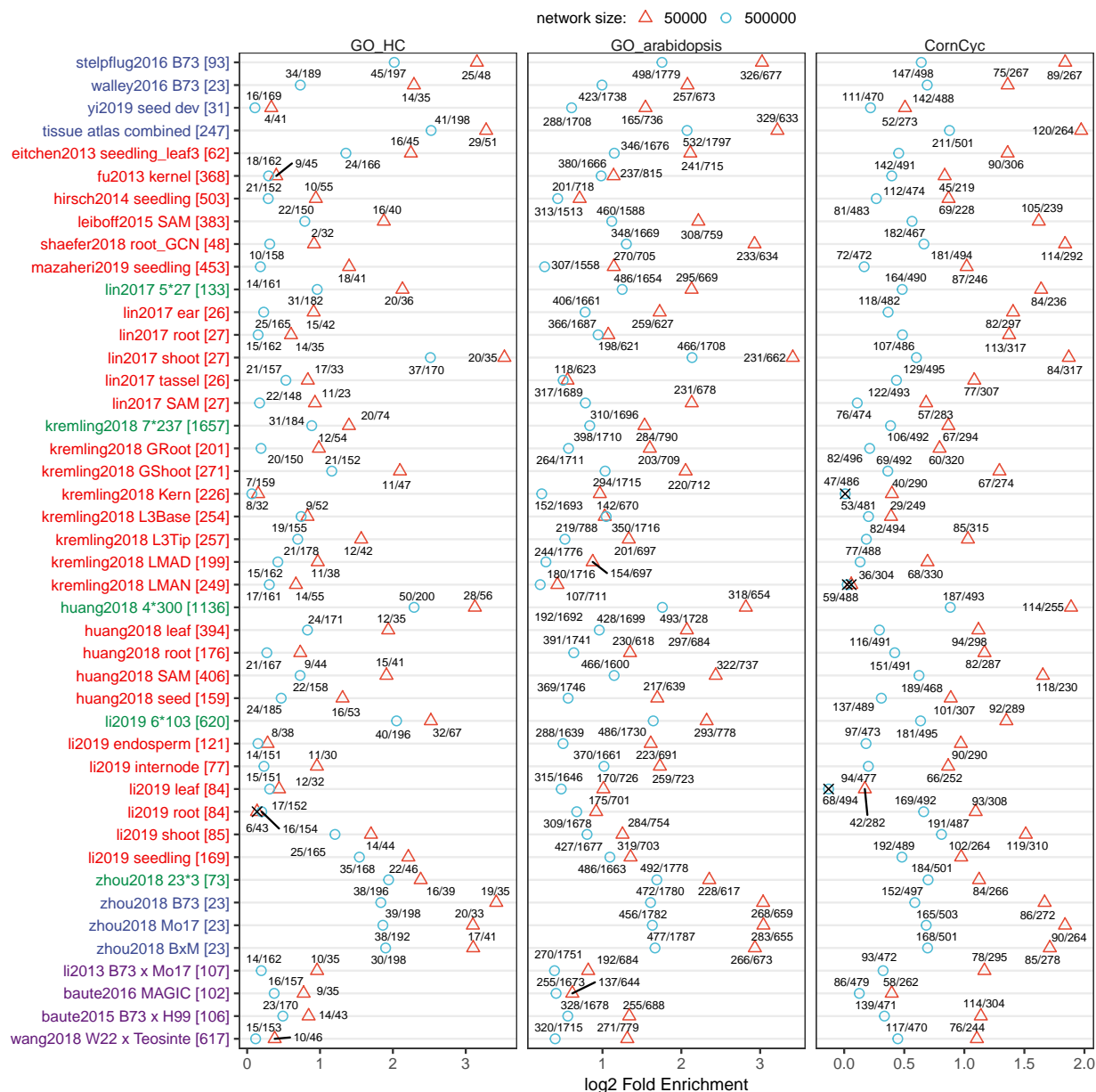
Figure 3. Enrichment of co-annotated GO/CornCyc terms in co-regulated network targets. For each network either the top 50,000 edges (red triangle) or 500,000 edges (blue circle) was taken to assess enrichment of GO/CornCyc annotation. Log2 fold enrichment is calculated as the observed number of shared GO/CornCyc terms (by targets regulated by a common TF) divided by the expected number of shared annotation terms (determined by permutation). The names for each of the networks are color coded to indicate B73 developmental surveys (blue), genotype surveys (red), meta-networks (green) or previously generated GRNs (teal).

Figure 4. Hierarchical clustering of 140 Gene Ontology (Uniprot.Plants) terms using log2 fold enrichment in different GRNs. Only GO terms enriched in at least 5 out of the 43 networks were used for clustering. Insignificant enrichment (p-value < 0.05) was treated as missing data and shown as white space in the figure.

Figure 5. TF-target validation of the combined tissue network in three selected natural variation datasets. Each panel shows the proportion of differentially expressed targets regulated by TFs showing different DE levels between two genotypes in one tissue/treatment condition. TF-target predictions were binned to 10 groups based on the interaction score in GRN. Each TF-target pair is classified according to the DE level of the TF ("non_DE", "DE1-2", "DE2-4", "DE4+" or "SPE") in each network. The proportion of TF-target pairs with the target also showing DE was then determined for each category. Dashed line in each panel represents the genome-wide (background) proportion of DE genes in each tissue/treatment setting.

Legend: non_DE · DE1−2 · DE2−4 · DE4+ · SPE

Baldauf2018 root1: B73 vs A554
Baldauf2018 root1: B73 vs H84
Baldauf2018 root1: B73 vs H99
Baldauf2018 root1: B73 vs Mo17
Baldauf2018 root1: B73 vs Oh43
Baldauf2018 root1: B73 vs W64A
Baldauf2018 root2: B73 vs A554
Baldauf2018 root2: B73 vs H84
Baldauf2018 root2: B73 vs H99
Baldauf2018 root2: B73 vs Mo17
Baldauf2018 root2: B73 vs Oh43
Baldauf2018 root2: B73 vs W64A
Baldauf2018 root3: B73 vs A554
Baldauf2018 root3: B73 vs H84
Baldauf2018 root3: B73 vs H99
Baldauf2018 root3: B73 vs Mo17
Baldauf2018 root3: B73 vs Oh43
Baldauf2018 root3: B73 vs W64A
Marcon2017 root_control: B73 vs Mo17
Marcon2017 root_drought: B73 vs Mo17
Sun2018 bract: B73 vs Mo17
Sun2018 endosperm: B73 vs Mo17
Sun2018 root: B73 vs Mo17
Sun2018 seedling: B73 vs Mo17
Sun2018 stem: B73 vs Mo17
Umn2014 seedling_cold: B73 vs B37
Umn2014 seedling_cold: B73 vs Oh43
Umn2014 seedling_control: B73 vs B37
Umn2014 seedling_control: B73 vs Oh43
Umn2014 seedling_heat: B73 vs B37
Umn2014 seedling_heat: B73 vs Oh43
Waters2017 leaf3_cold: B73 vs Mo17
Waters2017 leaf3_cold: B73 vs PH207
Waters2017 leaf3_control: B73 vs Mo17
Waters2017 leaf3_control: B73 vs PH207
Waters2017 leaf3_heat: B73 vs Mo17
Waters2017 leaf3_heat: B73 vs PH207
Weihmann2016 leaf: B73 vs GJ
Zhou2018 auricle: B73 vs Mo17
Zhou2018 blade_leaf: B73 vs Mo17
Zhou2018 coleoptile: B73 vs Mo17
Zhou2018 ear: B73 vs Mo17
Zhou2018 embryo: B73 vs Mo17
Zhou2018 endosperm14D: B73 vs Mo17
Zhou2018 endosperm27D: B73 vs Mo17
Zhou2018 flag_leaf: B73 vs Mo17
Zhou2018 floret: B73 vs Mo17
Zhou2018 husk: B73 vs Mo17
Zhou2018 internode: B73 vs Mo17
Zhou2018 kernel: B73 vs Mo17
Zhou2018 radicle_root: B73 vs Mo17
Zhou2018 root: B73 vs Mo17
Zhou2018 seed_imbibed: B73 vs Mo17
Zhou2018 seedling_leaf: B73 vs Mo17
Zhou2018 seedling_meristem: B73 vs Mo17
Zhou2018 seedling_root: B73 vs Mo17
Zhou2018 sheath: B73 vs Mo17
Zhou2018 silk: B73 vs Mo17
Zhou2018 spikelet: B73 vs Mo17
Zhou2018 tassel_stem: B73 vs Mo17
Zhou2018 tassel: B73 vs Mo17
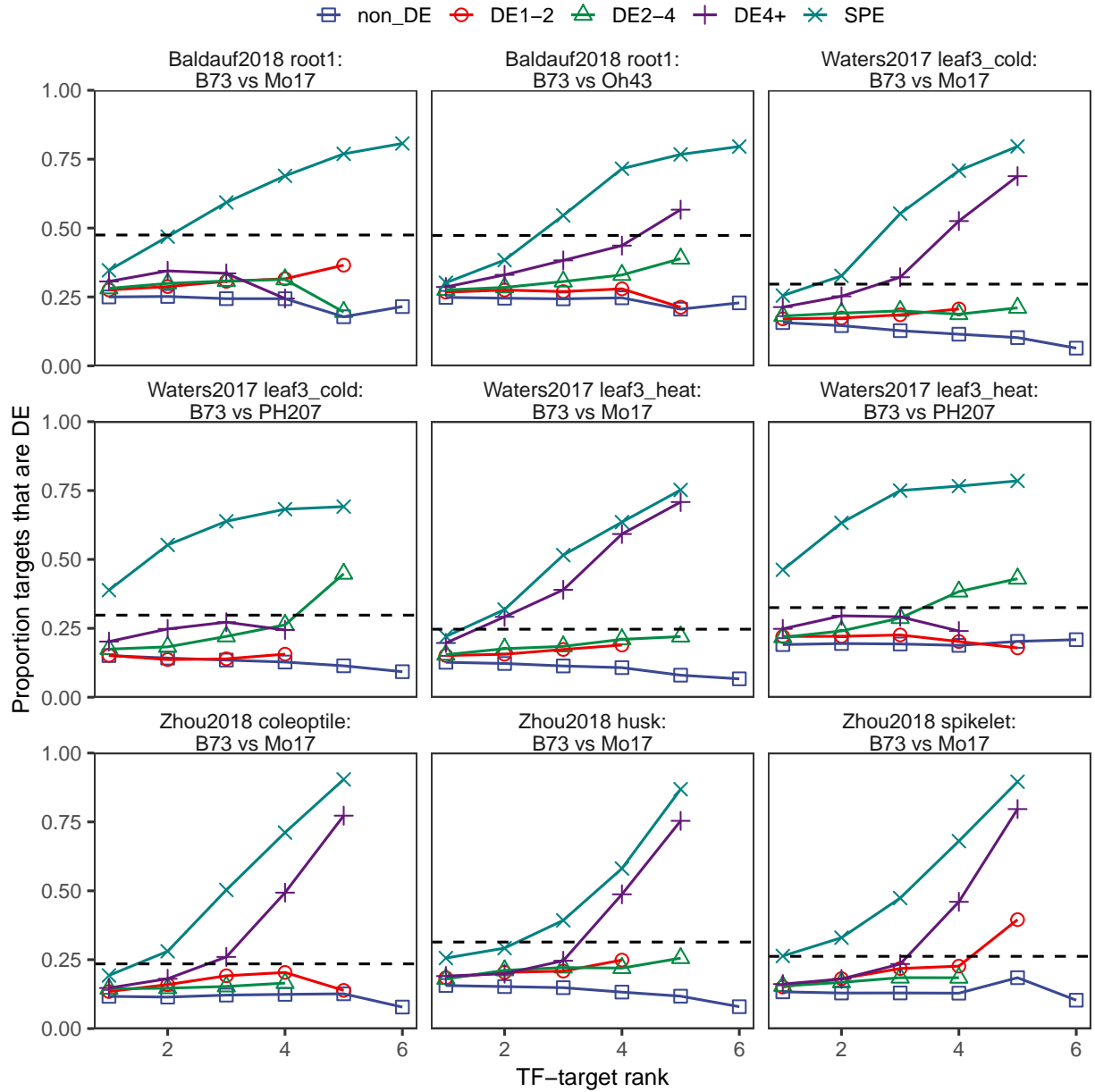
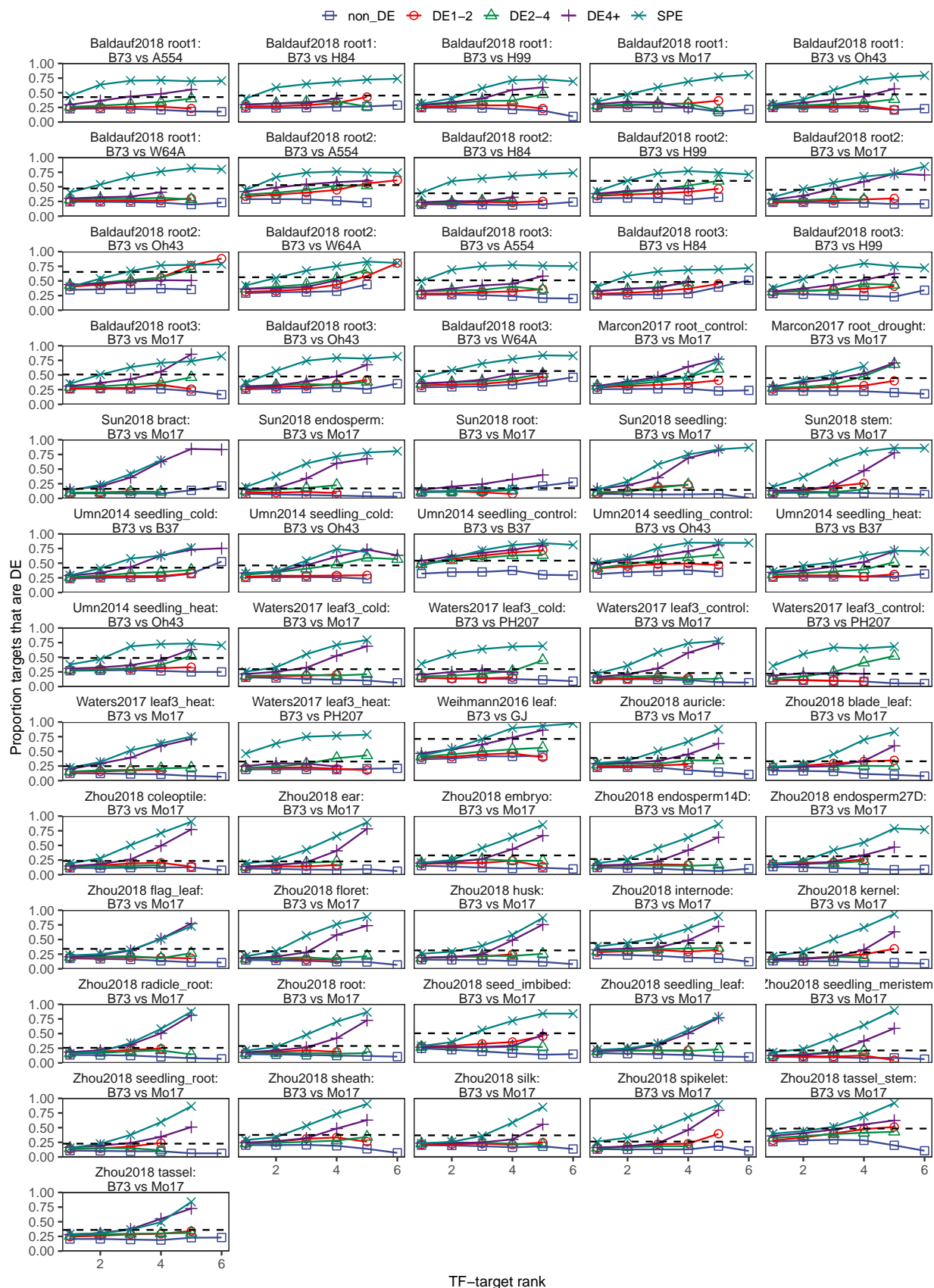Proportion targets that are DE

TF−target rank

Figure S8. TF-target validation of the combined tissue network in all six selected natural variation datasets. Each panel shows the proportion of differentially expressed targets regulated by TFs showing different DE levels between two genotypes in one tissue/treatment condition. TF-target predictions were binned to 10 groups based on the interaction score in GRN. Each TF-target pair is classified according to the DE level of the TF ("non_DE", "DE1-2", "DE2-4", "DE4+" or "SPE") in each network. The proportion of TF-target pairs with the target also showing DE was then determined for each category. Dashed line in each panel represents the genome-wide (background) proportion of DE genes in each tissue/treatment setting.

Figure 5B. Enrichment in differentially expressed targets regulated by TFs that show SPE patterns. Color and number in each cell represents the enrichment P-value (-log10 transformed, hypergeometric test p-value) of (SPE TF regulated) target DE proportions relative to the genome-wide proportion of DEGs for each GRN (row-wise) evaluated against a tissue/treatment condition in a natural variation dataset (column-wise). Only the top edges with rank 4 and higher were taken from each network.
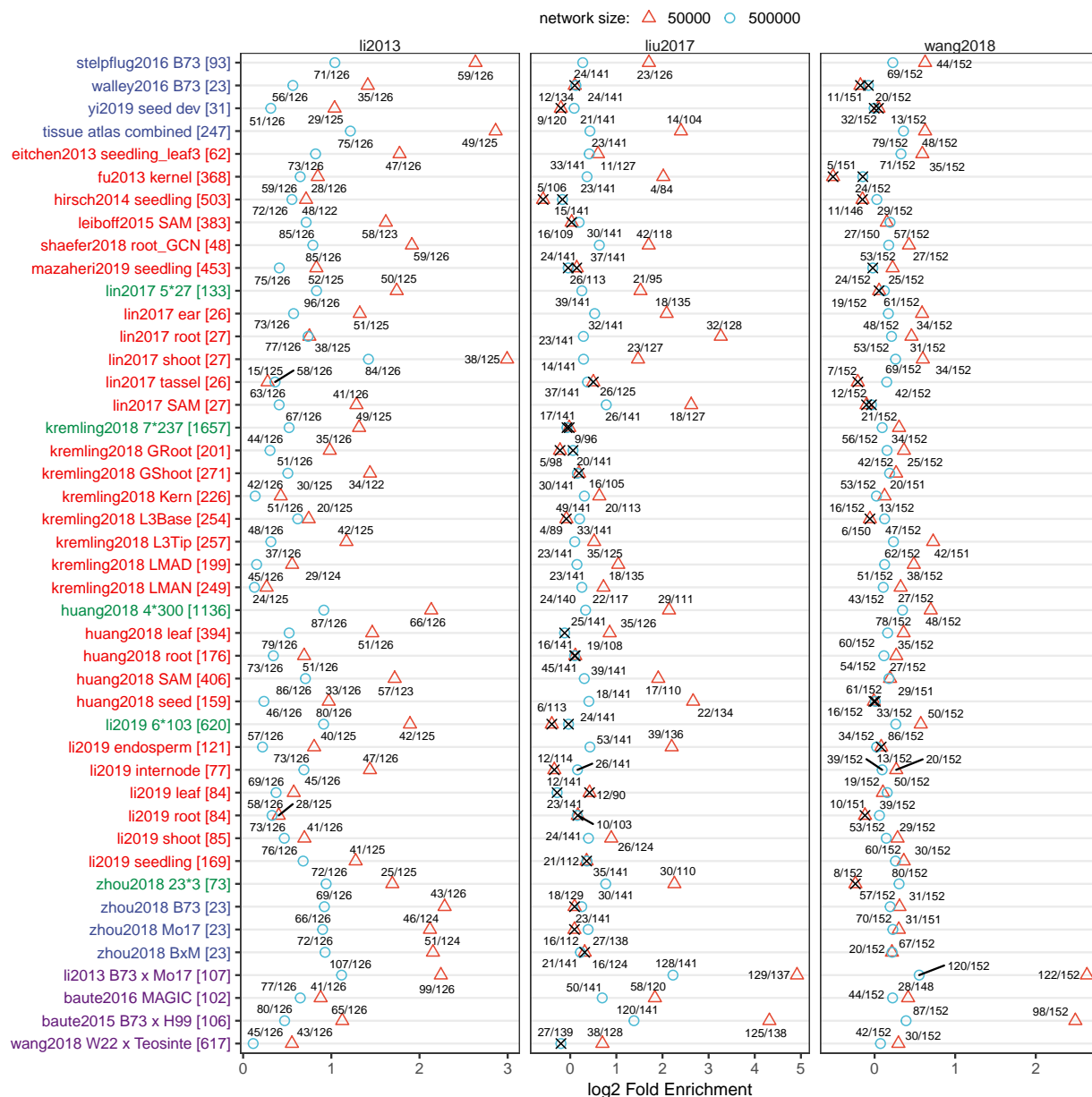
Figure S9. Enrichment of co-regulated targets between previously identified trans-eQTL hotspots and TF-target associations predicted by GRNs. For each network either the top 50,000 edges (red triangle) or 500,000 edges (blue circle) was taken to assess enrichment of co-regulation. Log2 fold enrichment is determined by the same permutation approach described in Figure 3.
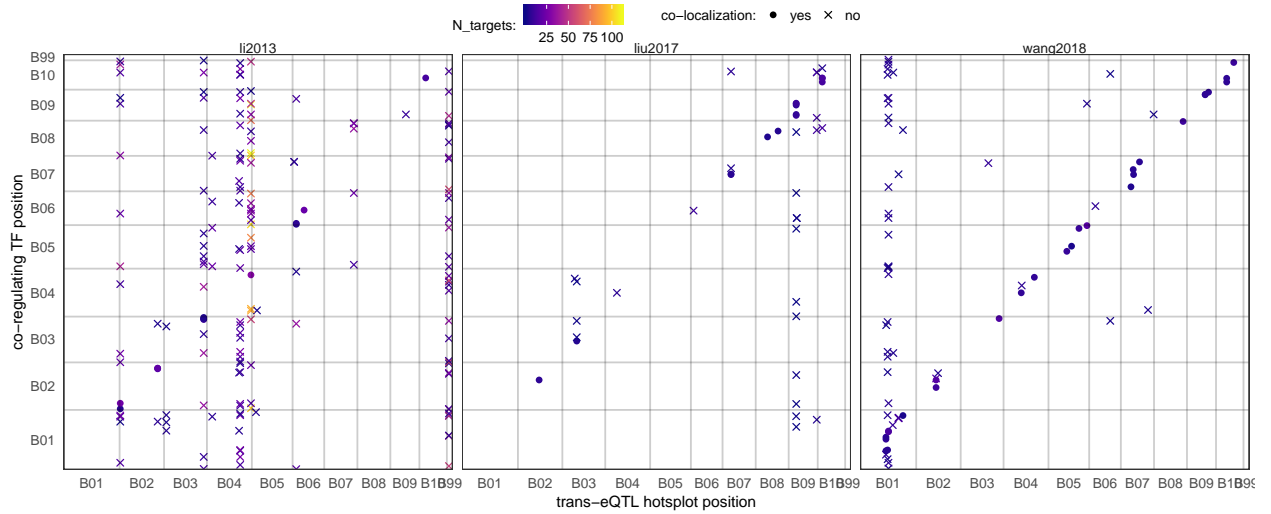
Figure S10. Co-localization of TFs predicted by GRNs in this study and trans-eQTL hotspots identified in previous studies that regulate the same set of targets. Each trans-eQTL hotspot were first tested for significant overlap in targets with any TFs (hypergeometric enrichment test as implemented in the phyper() function in R). To control for false positives, only TFs identified in at least two (out of 8 high quality networks, see Methods) that show significant co-regulation with at least one trans-eQTL hotspot (p < 0.01) were kept. Trans-eQTL hotspots identified in previous maize assemblies were lifted over to the AGPv4 assembly coordinates. Co-localization of a TF and a trans-eQTL is determined if the two coordinates are within 10-Mbp distance. Color of each dot represents the number of common targets between the predicted TF regulator and the trans-eQTL hotspot.

Figure 6. Identification of acting transcription factors underlying trans-eQTL hotspots identified in previous studies. (A) Co-localization of TFs predicted by GRNs in this study and trans-eQTL hotspots identified in previous studies that regulate the same set of targets. Each dot represents a TF supported by at least two high quality networks to show significant co-regulation with at least one trans-eQTL hotspot, and are within 10-Mbp distance from the trans-eQTL hotspot location; (B) Identification of R1 (colored, Zm00001d026147) co-localizing a previous trans-eQTL hotspot as the master regulator of the well studied anthocyanin biosynthesis pathway; (C) and (D) Identification of two previously uncharacterized TFs, the homeobox-transcription factor 87 (hb87, Zm00001d046405) and MYB-transcription factor 61 (myb61, Zm00001d053124) that co-localize previous trans-eQTL hotspots as the master regulator of the chlorophyllide biosynthesis pathway and the major CO2 fixation pathway (Calvin cycle pathway), respectively.